Biochimica et Biophysica Acta 1822 (2012) 150–160

Contents lists available at SciVerse ScienceDirect

Biochimica et Biophysica Acta

journal homepage: www.elsevier.com/locate/bbadis

Lysosomal vitamin E accumulation in Niemann–Pick type C disease

Luz Fernanda Yévenes [a,b], Andrés Klein [b], Juan Francisco Castro [b], Tamara Marín [b], Nancy Leal [a], Federico Leighton [c], Alejandra R. Alvarez [a,*], Silvana Zanlungo [b,d,**]

[a] Departamento de Biología Celular y Molecular, Facultad de Ciencias Biológicas, Pontificia Universidad Católica de Chile, Santiago, Chile
[b] Departamento de Gastroenterología, Facultad de Medicina, Pontificia Universidad Católica de Chile, Santiago, Chile
[c] Departamento de Fisiología, Facultad de Ciencias Biológicas, Pontificia Universidad Católica de Chile, Santiago, Chile
[d] Fondap-Center for Genome Regulation, Chile

ARTICLE INFO

Article history:
Received 23 June 2011
Received in revised form 4 November 2011
Accepted 9 November 2011
Available online 15 November 2011

Keywords:
Vitamin E
Niemann–Pick C
Cholesterol
Lysosomes

ABSTRACT

Niemann–Pick C disease (NPC) is a neuro-visceral lysosomal storage disorder mainly caused by genetic defects in the *NPC1* gene. As a result of loss of NPC1 function large quantities of free cholesterol and other lipids accumulate within late endosomes and lysosomes. In NPC livers and brains, the buildup of lipids correlates with oxidative damage; however the molecular mechanisms that trigger it remain unknown. Here we study potential alterations in vitamin E (α-tocopherol, α-TOH), the most potent endogenous antioxidant, in liver tissue and neurons from NPC1 mice. We found increased levels of α-TOH in NPC cells. We observed accumulation and entrapment of α-TOH in NPC neurons, mainly in the late endocytic pathway. Accordingly, α-TOH levels were increased in cerebellum of NPC1 mice. Also, we found decreased mRNA levels of the α-TOH transporter, α-Tocopherol Transfer Protein (α-TTP), in the cerebellum of NPC1 mice. Finally, by subcellular fractionation studies we detected a significant increase in the hepatic α-TOH content in purified lysosomes from NPC1 mice. In conclusion, these results suggest that NPC cells cannot transport vitamin E correctly leading to α-TOH buildup in the endosomal/lysosomal system. This may result in a decreased bioavailability and impaired antioxidant function of vitamin E in NPC, contributing to the disease pathogenesis.

© 2011 Published by Elsevier B.V.

1. Introduction

Niemann–Pick type C (NPC) disease, an autosomal recessive and neurodegenerative lipidosis, is mainly caused by mutations in the *NPC1* gene [1]. NPC1 participates in cholesterol trafficking and egress from the endosomal/lysosomal compartment to the cellular metabolic active pool [2–5]. *NPC1* mutations lead to accumulation of unesterified cholesterol and other lipids within lysosomes [6–10]. NPC patients present progressive neurodegeneration with increased apoptosis, especially of the cerebellar Purkinje cells [11–19]. Previous work from our group demonstrates that oxidative stress is the main upstream stimulus activating neuronal apoptosis in NPC neurons [19,20] and that oxidative damage is present in livers of NPC mice (unpublished results from our lab).

Vitamin E availability is crucial for antioxidant defenses in the organism. The most bio-active form of vitamin E is α-tocopherol (α-TOH) [21,22]. The cerebellum, which is one of the most afflicted brain areas in NPC disease, is particularly sensitive to oxidative damage. Recently, Ulatowski et al. have reported altered vitamin E status in NPC mice [23], suggesting that levels of this antioxidant could be involved in the pathological mechanisms of NPC disease.

Interestingly, vitamin E deficient mice present higher levels of neuroprostanes (a lipid peroxidation marker) in cerebellum compared with other zones of the CNS. This suggests that the cerebellum is more vulnerable to the lack of vitamin E than other brain areas [24]. Moreover, patients suffering from Ataxia with isolated Vitamin E Deficiency (AVED), a neurodegenerative disease with autosomal recessive inheritance caused by mutations in the *Ttpa* gene which encodes the α-TOH specific intracellular transporter [25,26], present sensory neurodegeneration and cerebellar ataxia, just as NPC patients do [26]. In AVED, there is an impairment of α-TOH incorporation into the VLDLs secreted by the liver, however the intestinal absorption of the dietary vitamin E and the packaging of α-TOH into chylomicrons are normal [25,26]. The murine model for this disease (*Ttpa* deficient

Abbreviations: NPC, Niemann–Pick type C disease; α-TOH, α-tocopherol (vitamin E); α-TTP, α-Tocopherol Transfer Protein; U18, U18666A drug; SHB, Sucrose-HEPES Buffer; RHN, Rat Hippocampal Neurons; *Ttpa*, gene encoding the α-TOH specific intracellular transporter

* Correspondence to: A.R. Alvarez, Facultad de Ciencias Biológicas, Pontificia Universidad Católica de Chile, Alameda 340, Casilla 114-D, Santiago, Chile. Tel.: +56 2 6862926; fax: +56 2 6862959.
** Correspondence to: S. Zanlungo, Facultad de Medicina, Pontificia Universidad Católica de Chile, Marcoleta 367, Casilla 114-D, Santiago, Chile. Tel.: +56 2 6863820; fax: +56 2 6397780.
E-mail addresses: aalvarez@bio.puc.cl (A.R. Alvarez), silvana@med.puc.cl (S. Zanlungo).

0925-4439/$ – see front matter © 2011 Published by Elsevier B.V.
doi:10.1016/j.bbadis.2011.11.009

mice) shows ataxia and retinal degeneration after the first year of life, symptoms can be reversed by vitamin E dietary supplementation [27]. NPC mice locomotor skills are slightly improved with vitamin E dietary supplementation [28] even though the mice present a high oxidative damage. NPC patients present decreased antioxidant capacity (expressed as Trolox equivalents) and reduced Coenzyme Q10 in serum, which indicates a decrease in the antioxidant defenses [29]. Therefore, is possible that the minimal improvements observed by vitamin E treatments in NPC mice are due to its decreased bioavailability in the NPC cells.

Due to its lipid nature, α-TOH intracellular transport requires the activity of several proteins that could also participate in the cholesterol trafficking pathways [30–36]. Furthermore, NPC1L1 protein, which has extensive homology with NPC1 [37], participates in α-TOH and cholesterol transport into enterocytes. Also this process is inhibited by ezetimibe, a well known inhibitor of cholesterol absorption [38–42].

Based on these antecedents we propose that the NPC1 transport pathway participates in α-TOH intracellular trafficking. We found increased α-TOH staining levels in 8 week-old NPC1 mice cerebellum compared to WT mice that correlates with increased levels of several oxidative stress markers, including expression levels of some classic oxidative stress response genes and nitrotyrosine, findings that were previously reported by our group [20]. Moreover, we observed accumulation and entrapment of α-TOH in NPC neurons, mainly in the late endocytic pathway. Accordingly, we observed an increase in α-TOH levels in NPC1 mice cerebellum. Furthermore, we have found decreased mRNA levels of the α-TOH transporter, α-Tocopherol Transfer Protein (α-TTP), in the cerebellum of NPC1 mice. Finally, by subcellular fractioning studies we found an increase in the hepatic α-TOH content in purified lysosomes from NPC1 mice. Together these results strongly suggest vitamin E trafficking alterations in NPC cells that lead to vitamin E accumulation and entrapment into the endocytic pathway which may result in a decreased bioavailability and antioxidant function of vitamin E in other cell compartments, contributing to the pathology of NPC disease.

2. Materials and methods

2.1. Animals

Sprague–Dawley rats were obtained from the animal facility of our Biological Science Faculty. BALB/c mice carrying a heterozygous mutation in the *Npc1* gene were kindly donated by Dr Peter Pentchev. *Npc1*$^{+/+}$ (Wild-type; WT) and *Npc1*$^{-/-}$ (NPC1) genotypes were identified using a PCR-based screening as described previously by Amigo et al. [43]. WT and NPC1 male mice of 6 and 8 week-old were used in the experiments. All protocols were approved by our institution's review board for animal studies and were in agreement with the US Public Health Service Policy on Humane Care and Use of Laboratory Animals recommended by the Institute for Laboratory Animal Research in its Guide for Care and Use of Laboratory Animals.

2.2. Primary rat and mice hippocampal cell culture

Hippocampi from Sprague–Dawley rats and NPC1 mice at embryonic day 18 were dissected, and primary hippocampal cultures were prepared as described by Alvarez et al. [44]. Hippocampal cells were seeded in poly-lysine-coated wells and maintained in Neurobasal medium supplemented with B27 (Invitrogen, Carlsbad, CA, USA) plus antibiotics (100 U/ml penicillin and 100 μg/ml streptomycin) for 5 days before the cell treatments. Glial proliferation was inhibited by adding 2 μM Cytosine-Arabinoside (AraC) on the second day and removed the next day.

2.3. U18666A treatment

Five days (DIV) cultured rat hippocampal cells were treated with U18666A (Enzo Life Sciences Inc. Farmingdale, NY) at 0.5 μg/ml for 24 h.

2.4. Filipin staining

Cells were fixed in 4% paraformaldehyde/4% sucrose in PBS for 30 min. After, cells were washed with PBS and treated with 2.5 mg/ml glycine for 20 min. Finally cells were treated with 25 μg/ml Filipin (Sigma Chemicals Co, St. Louis, MO) for 30 min, washed with PBS and covered with Fluoromount-G (SouthernBiotech, Birmingham, AL, USA). Images were captured with an Olympus BX51 microscope (Olympus, Tokyo, Japan) and analyzed with the Image-Pro Express program (Media Cybernetics, Bethesda, MD, USA).

2.5. Immunofluorescence on coverslips

Hippocampal cells were plated on poly-lysine-coated coverslips (30,000 cells/cover). After 6 days in Neurobasal/B27, prior fixation and immunostaining, the cells were stained with LysoTracker Red (1 μM; DND-99, Invitrogen, Carlsbad, CA) for 2 h at 37 °C. Later, the cells were fixed in 4% paraformaldehyde/4% sucrose in PBS and permeabilized with 0.02% Triton X-100. Then, cells were blocked with 5% horse serum in PBS. Immunostaining was done using anti-Lamp1 (1:250; 1D4B, Abcam, Cambridge, MA), anti-TfR (1:120; Zymed, Invitrogen Detection Technologies, Carlsbad, CA), and anti-α-TOH (1:500; US Biological, Swampscott, MA). Anti-rabbit-Alexa Fluor-488 (1:5000), anti-mouse-Alexa Fluor-594, anti-mouse-Alexa Fluor-488 (1:5000) and streptoavidin-Alexa Fluor-488 (1:1000) from Molecular Probes, Invitrogen Detection Technologies, Carlsbad, CA, were used as secondary antibodies. Fluorescent images were captured with a confocal Olympus microscope or with an Olympus BX51 microscope (Olympus, Tokyo, Japan) and analyzed with the Image-Pro Express program (Media Cybernetics, Bethesda, MD, USA). The results are shown as the average of 3 independent experiments per condition. Colocalization analyses were done as follows: Images were captured with a confocal Olympus microscope using a 100× objective with a 1.4 numerical aperture and 0.3 μm successive focal planes. The out-of-focus light was removed by a 3D iterative deconvolution algorithm and the Mander's coefficients were determined using the JACoP application (ImageJ).

For pixel quantification the Multi Measure application (ImageJ) was used. For cellular culture images quantification each neuron was taken as an independent region of interest (ROI). Then each ROI was averaged and divided by the total number of quantified neurons. For tissue images, the whole image was taken as a ROI and a basal intensity was determined and used as a threshold for all the images; then, the final intensities were averaged and divided by the quantified area.

2.6. Tissue immunofluorescence procedures

Mice (6 and 8 week-old) were anesthetized with xylazine/ketamine (0.12 and 0.8 mg/10 g body weight, respectively) and perfused with 4% paraformaldehyde in PBS. Cerebellum and livers were removed and postfixed overnight at 4 °C, followed by 30% sucrose in PBS at 4 °C overnight, then were cut in 40 μm coronal sections and 12 μm sections, respectively, with a cryostat (Leica CM1850) at −20 °C. 4–5 slices by animal were stained by experiment. We examined at least 4 animals per condition.

For immunofluorescence the specific antibodies used were: anti-Cathepsin B (1:200), anti-Calbindin (1:100) from Sigma Chemicals Co, St. Louis, MO; anti-α-TOH (1:500; US Biological, Swampscott, MA) and Phalloidin-TRITC (1:1000; Invitrogen, Carlsbad, CA). The

slices were incubated with primary antibodies in PBS with 0.2% gelatin/0.4% TritonX-100 in PBS, then slices were incubated with secondary antibodies anti-rabbit-Alexa Fluor-488 (1:5000); anti-mouse-Alexa Fluor-594, anti-mouse-Alexa Fluor-488 (1:5000) and anti-goat-Alexa Fluor-633 (1:5000) from Molecular Probes, Invitrogen Detection Technologies, Carlsbad, CA. Fluorescent images were captured with a confocal Olympus microscope or with an Olympus BX51 microscope (Olympus, Tokyo, Japan) and analyzed with Image-Pro Express (Media Cybernetics, Bethesda, MD, USA). The images in a given experiment were always acquired using the same parameters.

2.7. Real-time PCR analysis

Total RNA from cultured rat hippocampal cells, cerebellum and liver was extracted, pretreated with DNAse (Invitrogen), and then reverse transcribed to cDNA using random primers (Invitrogen). Real-time PCR was then performed (model AB7500, Applied Biosystems, Foster City, CA, USA). The PCR conditions and the gene-specific primer sequences are provided in the supplementary material section. Expression in mice tissue and rat hippocampal cells were normalized using the 18S gene. Data from the PCR reactions were analyzed using the mathematical model described by Pfaffl [45].

2.8. Mice liver lysosomes isolation

Livers were homogenized in 4 ml of SHB (20 mM HEPES pH 7.2; 320 mM sucrose; 1 mg/ml Leupeptin, 1 mM PMSF and 1% NAC). Tissues were mechanically homogenized using a glass/teflon Potter Elvejhem homogenizer and kept at 4 °C. A sample of each fraction, including the homogenate, was stored to be used for the α-TOH content determination by HPLC-EC. The homogenates then were diluted to 10 ml with SHB and centrifuged at 2500 rpm for 10 min. The supernatant was removed (Extract 1) and the pellet was resuspended in 5 ml of SHB, and centrifuged at 2200 rpm for 10 min. Pellets were discarded and the obtained supernatant (Extract 2) was mixed with the Extract 1 (Total Extract). Total Extracts were centrifuged at 2200 rpm for 10 min. Pellets (Nuclear Fraction) were resuspended in 1 ml of SHB and the supernatants were centrifuged at 8000 rpm for 10 min. The new pellets (Mitochondrial Fraction) were resuspended in 1 ml of SHB and the supernatants were centrifuged at 12,000 rpm for 45 min. The obtained pellets (Lysosomal Fraction) were resuspended in 1 ml of SHB and supernatants (Soluble Proteins) were stored. All the procedures were done at 4 °C and for the centrifugations a Sorvall centrifuge with a Sorvall SM-24 rotor was used (Thermo Fisher Scientific Inc., Waltham, MA, USA).

2.9. HPLC-EC α-TOH content measurements

Samples of approximately 0.075 g of frozen tissue (brain, cerebellum and liver) were mechanically homogenized, placed in 0.5 ml homogenization buffer (20 mM Tris pH 7.2; 2 mM MgCl2; 0.25 M sucrose; 1 mg/ml Leupeptin; 1 mM Pepstatin; 1 mM PMSF and 0.1% BHT) and were mechanically homogenized. Tissues were mechanically homogenized using an Ultraturrax (Kinematica, Littau, Suiza). Protein concentration was measured as described by Bradford [46]. α-TOH content was determined by reverse phase HPLC-EC as described by Motchnik et al. [47]. Briefly, a 100 μl sample was resuspended in ethanol and mixed briefly. Afterwards, hexane was added. The solution was mixed, centrifuged for 15 min at 1000 *g*, and the upper hexane layer was transferred to a glass tube; the hexane extraction procedure was repeated twice. Hexane extracts were pooled and dried at room temperature under a stream of nitrogen, and the resulting pellet was dissolved in methanol/ethanol (1:1, v/v). Samples were then separated in columns using 20 mM Lithium Perchlorate in methanol/H_2O (96:4, v/v) as mobile phase.

2.10. Statistical analysis

Mean and standard error of the mean values with the corresponding number of experiments are indicated in the figure legends. Probability values of the data for Student t-tests and ANOVA tests with Bonferroni's post-test were obtained using the GraphPad Prism 5 (Graph Pad Software, Inc., San Diego, USA).

3. Results

3.1. U18666A treatment triggers cholesterol and α-TOH accumulation

We treated primary rat hippocampal neurons with U18666A (U18) using a concentration of 0.5 μg/ml for 24 h as previously described by Karten et al. [48] and us [20]. As expected, this drug induced intracellular cholesterol accumulation (assessed by filipin staining and cellular cholesterol content measurement) (Fig. 1A and

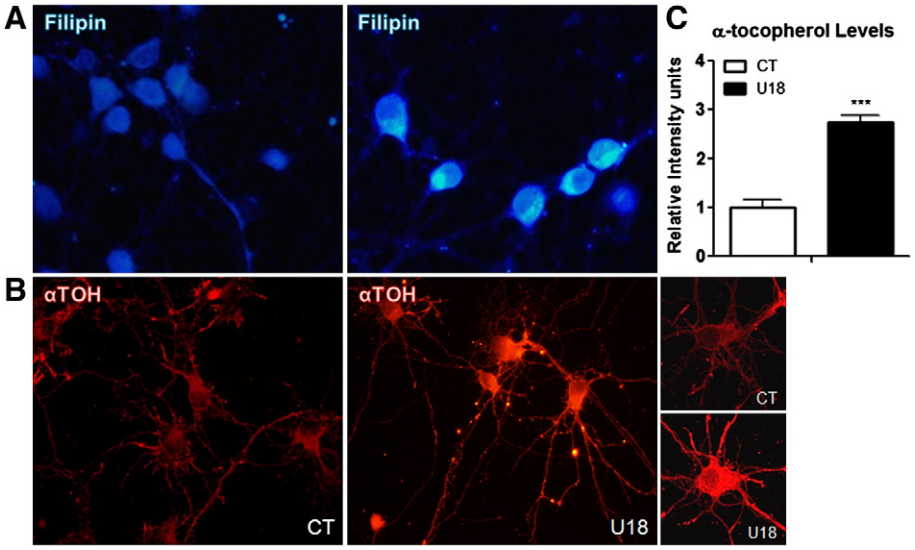

Fig. 1. U18666A-induced α-tocopherol accumulation in neurons. Control (CT) and U18666A (U18)-treated (0.5 μg/ml for 24 h) rat hippocampal neurons were fixed, and cholesterol and α-tocopherol (αTOH) accumulation was detected by filipin staining (A) and immunofluorescence (B), respectively. Image size: 3.6 pixels/nm. Amplifications of α-TOH immunofluorescence are shown (magnification: 2). (C) The quantitation of α-TOH fluorescence intensity of 7 images. Results are shown as mean ± SEM. *** $p<0.001$.

Supplementary Data) without inducing cell death (see Supplementary Data).

Next we characterized the commercial antibody against BSA/α-TOH and demonstrated its specificity (see Supplementary Data). Since this antibody has a high affinity for α-TOH we used it to assess the cellular levels of α-TOH by immunofluorescence. With this antibody we found a 3-fold increment of the α-TOH signal in U18-treated neurons compared to control (untreated) neurons (Fig. 1B and C).

This warranted further investigation. To determine the subcellular localization of α-TOH in the U18-treated neurons we performed double immunofluorescences against α-TOH and: i) transferrin receptor (TfR, early and recycling endosomes marker); ii) Lamp1 (endosomes and lysosomes marker) and; iii) LysoTracker (lysosomes marker) (Fig. 2A). By colocalization analyses, using Mander's coefficients which measure the proportion of overlapping signal of each channel with the other, we determined the proportion of vesicles that contain α-TOH (left axis, Fig. 2B) and the proportion of total intracellular α-TOH contained within vesicles (right axis, Fig. 2B). The right axis value will be higher if there is more α-TOH contained within the respective vesicles and the left axis value will be higher if there are a greater number of vesicles that contain α-TOH. We found that α-TOH was distributed between all the compartments (Fig. 2B). For the TfR positive vesicles, both ratios were similar (Fig. 2B, red bars). The Lamp1 positive vesicles contained more α-TOH from its total compared with other compartments (Fig. 2B, hatched blue bar) even though not all Lamp1 positive vesicles contained α-TOH (Fig. 2B, blue bar). Finally, for the LysoTracker positive vesicles the proportion of vesicles from the total pool that contained α-TOH (Fig. 2B, green bar) was greater than the proportion of the total α-TOH contained within the LysoTracker positive vesicles (Fig. 2B, green hatched bar). In conclusion, α-TOH accumulates mainly in Lamp1 positive vesicles; however, almost all LysoTracker positive vesicles contain α-TOH. Nonetheless, we cannot discard the presence

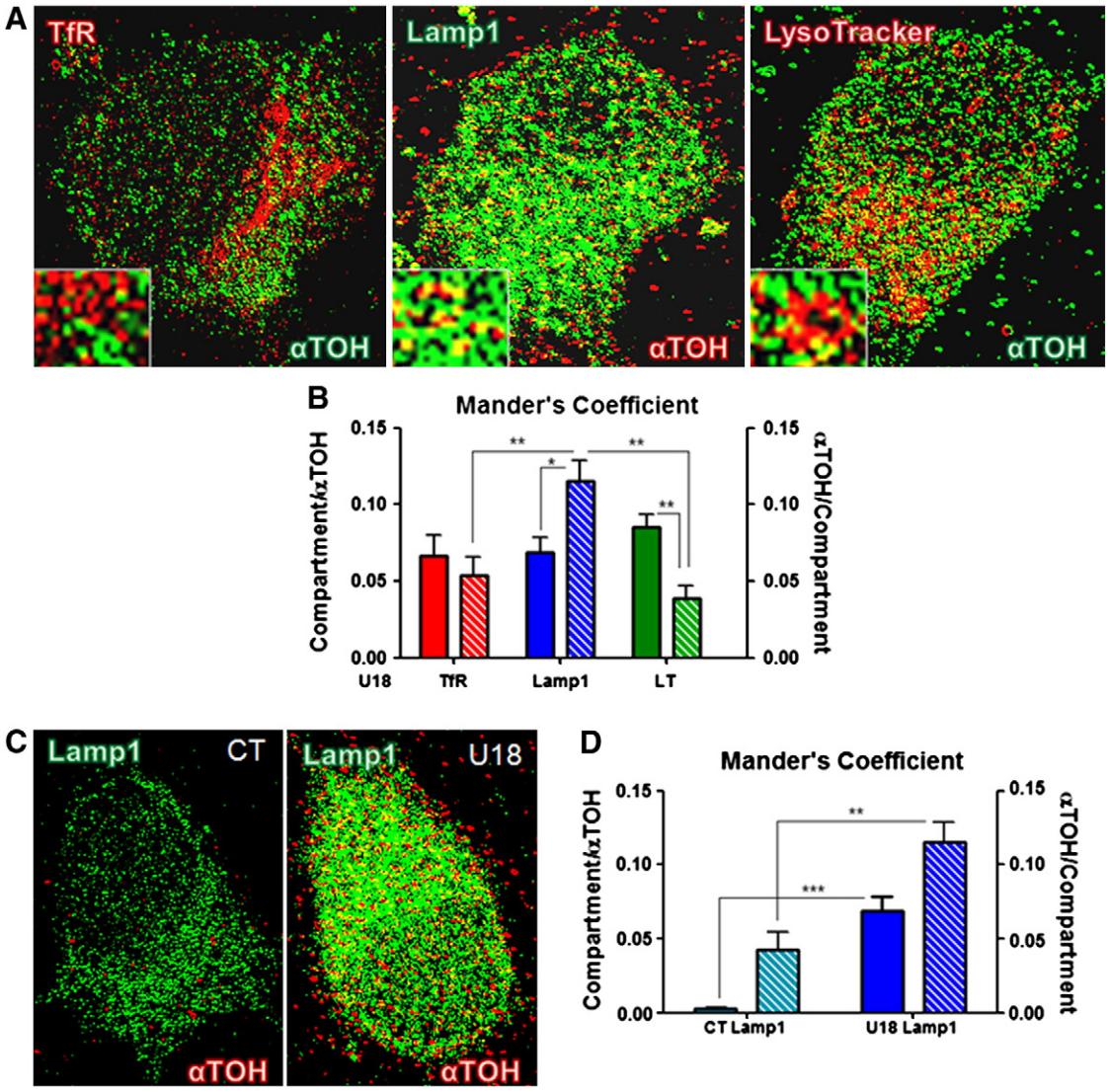

Fig. 2. Colocalization analysis between α-tocopherol and endocytic pathway markers in U18666A-treated neurons. A. Confocal fluorescence images showing α-TOH (green) and the Transferrin Receptor (red) immunofluorescences (TfR, left), α-TOH (red) and Lamp1 (green) immunofluorescences (center) and α-TOH (green) immunofluorescence with the lysosomal marker LysoTracker (red) of U18666A-treated rat hippocampal neurons (0.5 μg/ml for 24 h). Image size: 5.6 pixels/nm. The lower left corner in each figure shows a magnification of the cytoplasm. Magnification: 7.9. B. Quantitation of the colocalization between α-TOH and the different markers of the endocytic pathway through Mander's coefficients of 5 images. The value of the not hatched bar corresponds to the left axis and the hatched bar corresponds to the right axis. Results are shown as mean ± SEM. * $p<0.05$; ** $p<0.01$. C. Confocal fluorescence images showing Lamp1 (green) and α-TOH (red) immunofluorescences of Control (CT) and U18666A-treated rat hippocampal neurons (0.5 μg/ml for 24 h). Image size: 5.6 pixels/nm. D. Quantitation of the colocalization between α-TOH and Lamp1 through Mander's coefficients of 5 images. The value of the not hatched bar corresponds to the left axis and the hatched bar corresponds to the right axis. Results are shown as mean ± SEM. ** $p<0.01$; *** $p<0.001$.

of α-TOH in other compartments that we have not evaluated, such as the mitochondria.

When we compared α-TOH colocalization with Lamp1 in control and U18-treated neurons (Fig. 2C), we found that a significant increase in both Mander's coefficients occurred. This result indicates that U18 treatment increases the number of Lamp1 positive vesicles that contain α-TOH (Fig. 2D, non-hatched bars) and an increase in the amount of α-TOH localized within those vesicles (Fig. 2D, hatched bars). This result suggests that the U18 treatment induces α-TOH accumulation in late endosomes.

3.2. α-TOH accumulation in NPC1 deficient primary neurons

After these analyses in the pharmacological model of NPC we focused our study in the genetic model of the disease, the BALB/c npc^{nih} mice (NPC1 mice). As previously described [13], NPC1 neurons presented morphological abnormalities with thicker and shorter prolongations, an enlarged axon shaft and ectopic dendrites (Fig. 3). As expected, NPC1 hippocampal neurons accumulated intracellular cholesterol, determined by filipin staining (Fig. 3D). As a control we performed immunofluorescences against NPC1 and, as expected, we found no signal in the NPC1 neurons (Fig. 3E). More importantly, when we evaluated α-TOH levels by immunofluorescence we found that the α-TOH signal was increased in NPC1 neurons compared with wild-type (WT) neurons (Fig. 3C and F).

3.3. Cerebellar α-TOH accumulation in NPC1 mice

The most affected organ in NPC disease is the cerebellum. Therefore, we performed double immunofluorescences against α-TOH and calbindin, a marker for Purkinje cells (Fig. 4). As expected, the NPC1 cerebellum tissue was deteriorated compared with the WT cerebellum tissue in the 6 and 8 week-old mice (Fig. 4B, E and H). This was evidenced by the disorganization of the cerebellum tissue as ectopic calbindin positive cells appeared in the nuclear and granular layer in the 8 week-old NPC1 mice (Fig. 4H). There was also a loss in the number of Purkinje cells in the 6 week-old NPC1 mice which was even greater in the 8 week-old NPC mice (Fig. 4B, E and H). More significantly, α-TOH levels were increased in the cerebellum of the NPC1 mice (Fig. 4A, D and G). When we compared the cerebella from 6 week-old NPC1 mice versus 8 week-old NPC1 mice we noticed Purkinje cells loss and ectopic calbindin positive neurons in 8 week-old mice tissue. Even though, a sub-set of calbindin positive neurons remained positive for α-TOH in 8 week-old NPC1 mice (Fig. 4D–I).

3.4. Hepatic α-TOH accumulation in NPC1 mice

Livers are severely damaged in NPC disease [1]. To study possible hepatic α-TOH alterations we performed triple immunofluorescences against α-TOH, cathepsin B and actin in liver slices from 6 and 8 week-old WT and NPC1 mice (Fig. 5A). NPC1 livers showed abnormal actin distribution with irregular cellular morphology, both indicators of tissue damage. These results agree with previously published data showing marked accumulation of multiple non-enzymatically formed cholesterol oxidation products in livers of 9 week-old NPC1 mice in comparison with wild-type mice, indicating the presence of oxidative stress in this tissue [49].

This was especially highlighted in 8 week-old NPC1 mice (Fig. 5A). We found an increase in cathepsin B levels in NPC mice liver and, interestingly, there was also a significant increase in α-TOH levels in the 6 week-old NPC mice (Fig. 5A and B). We could not detect significant differences between 8 week-old WT and NPC1 mice, probably because of the high extent of NPC1 liver damage. Finally, we found an increase in the colocalization between α-TOH and cathepsin B in the 6 week-old NPC1 mice, suggesting that α-TOH accumulates in the late endosomal/lysosomal compartment (Fig. 5C).

3.5. Changes in α-TOH content and mRNA expression of α-TOH-metabolism and transport related genes in NPC1 mice

To determine α-TOH concentration in different organs we used HPLC-EC (Fig. 6). Although we did not detect changes in α-TOH concentration in the brain and plasma of 8 week-old mice (Fig. 6A and B), we found a significant increase in the cerebellar α-TOH levels of NPC1 mice (Fig. 6A). Hepatic NPC1 α-TOH levels were higher than WT, but not significantly. This tendency was more pronounced in the 6 week-old NPC1 tissue (Fig. 6C), in concordance with our immunofluorescence results.

The differences observed in α-TOH levels in the NPC1 mice tissues may be related to changes in the expression of key genes that participate in the transport and metabolism of α-TOH. Therefore, we measured the expression of several α-TOH -related genes in the cerebellum and liver of WT and NPC1 mice.

We found that *Srbi* mRNA levels are elevated in the liver of the 8 week-old NPC1 mice (Fig. 7B) and that there is a trend to be elevated in the liver at 6 weeks (Fig. 7B) that can be also observed in the cerebellum of the 8 week-old NPC1 mice (Fig. 7A). These increments suggest that there is an increased uptake of α-TOH into the liver and cerebellum [32].

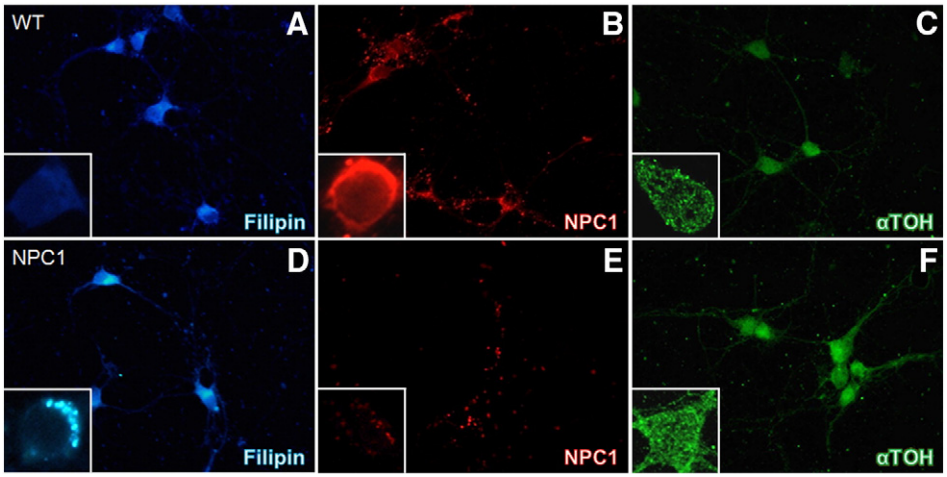

Fig. 3. Intracellular accumulation of α-tocopherol in NPC1 mice hippocampal neurons. Wild-type (WT) and *Npc1*$^{-/-}$ (NPC1) mice hippocampal neurons were stained with filipin (blue; A, D), immunostained with anti-NPC1 (red; B, E) and anti-α-TOH (green; C, F). Image size: 3.6 pixels/nm. Amplifications of each condition are shown in the left corner (magnification: 2.9).

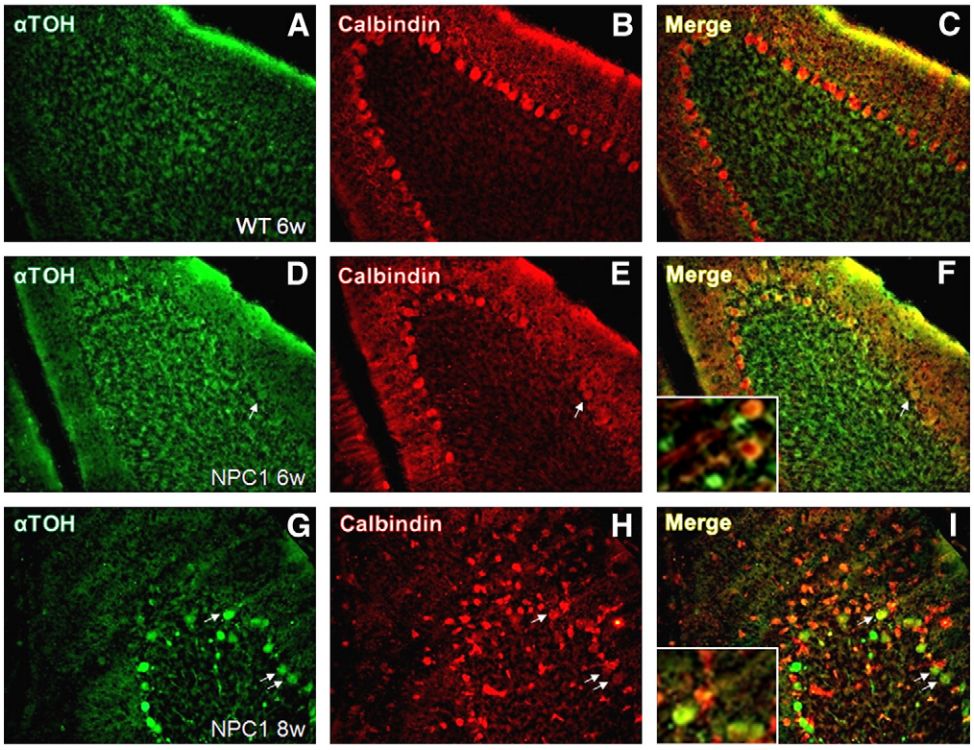

Fig. 4. Immunofluorescence analysis for α-tocopherol signal in the cerebellum of WT and NPC1 mice. Representative immunofluorescence images for α-TOH (A, D, G) and calbindin (B, E, H) in cerebellum of 6 and 8 week-old (6w and 8w), wild-type (WT) and *Npc1*$^{-/-}$ (NPC1) mice are shown. In C, F, and I the merge of both signals is shown. Image size: 3.6 pixels/nm. Amplifications for 6w and 8w NPC1 mice merge images are shown in the left corner (magnification: 1.9).

For the α-TOH specific transporter α-TTP, we found a significant reduction in *Ttpa* mRNA levels in the cerebellum of 6 week-old NPC1 mice in comparison with the WT mice (Fig. 7C), which correlated with the increase in cerebellar α-TOH levels of NPC1 mice (Fig. 6A). Nonetheless, we did not find differences between WT and NPC1 mice 8 week-old (Fig. 7C), even though at this age α-TOH cerebellar levels were increased in the NPC1 mice (Fig. 4A and G). On the other hand, no differences were found in the hepatic *Ttpa* mRNA levels between WT and NPC1 mice both at 6 and at 8 weeks of age (Fig. 7D). However there was a slight trend to be increased in NPC1 mice at 6 weeks of age, in which there was an increase in the levels of the α-TOH levels (Figs. 7D, 6C and 5). In addition we measured *Ttpa* levels in untreated and U18-treated rat hippocampal neurons and found no differences between both groups (Fig. 7E) despite the increase of the α-TOH levels in the U18-treated neurons (Fig. 1B and C).

We also measured the mRNA levels of another intracellular α-TOH transporter, *Sec14l2* (Fig. 7F and G), and we found that its expression is slightly incremented in the liver of the 6 week-old NPC1 mice, (Fig. 7G) which suggests that part of the internalized α-TOH could be transported into the Golgi apparatus and mitochondria [50].

In agreement with previously published data we found an increase in *Apoe* mRNA levels in cerebellum of 8 week-old NPC1 mice (Fig. 7H) [51]. *Apoe* is expressed in the cells of the CNS, particularly in astrocytes and increases its expression following nerve damage [52]. Therefore, it is possible to speculate that increase in *Apoe* expression in NPC1 mice cerebellum is related to the transport of cholesterol and tocopherol toward damaged neurons.

Published data from Abe et al. [53] suggests that lipolysis of triacylglycerol-rich chylomicron by LPL is necessary for postprandial vitamin E transport to the liver and subsequent transport to the other tissues. We found that *Lpl* levels are increased in the liver of the 6 and 8 week-old NPC1 mice (Fig. 7K), there are also significantly elevated in the cerebellum of the 8 week-old NPC1 mice while there is a trend to be elevated at 6 week-old NPC1 mice (Fig. 7J). Interestingly, LPL is also active in the CNS and expressed in Purkinje cells of the cerebellum. Moreover, CNS LPL is functional mediating the uptake of triglyceride fatty acids throughout the CNS [54].

These results suggest increased α-TOH and fatty acids transport to the liver and cerebellum of the NPC1 mice.

3.6. Elevated levels of α-TOH in lysosomal fractions from NPC1 mice livers

Finally, to corroborate our staining analysis biochemically and determine the α-TOH concentration in different organelles, we performed subcellular fractionation followed by HPLC-EC analysis on 6 week-old WT and NPC1 mice livers. We choose this time point because we found the biggest differences in hepatic α-TOH concentration at this stage (Figs. 5 and 6C). α-TOH was increased in every fraction measured (2-fold increase in the extract and in the mitochondrial fraction) in the NPC1 tissue. But, there was a 3-fold increase of α-TOH levels in the lysosomal fraction of the NPC1 tissue (Fig. 8). This result confirms that α-TOH accumulates mainly in the late endosomal/lysosomal compartment in the NPC1 cells.

4. Discussion

Our results show a buildup of vitamin E in the endo/lysosomal system in NPC models, suggesting impairments in vitamin E bioavailability and antioxidant capacity. Deficiencies in the NPC1 protein impair cholesterol transport from the endo/lysosomal system to other organelles [6–10]. Our results suggest that NPC1 function is also relevant for intracellular transport of vitamin E in the endocytic pathway.

Our findings are in agreement with a recently published report that describes lysosomal NBD-tocopherol accumulation in human NPC1 mutant fibroblasts and hepatocyte cell lines with NPC1 or NPC2 knock-down [23]. That report also found increments in vitamin E content in livers of NPC1 and NPC2 mice at 12 week-old and in

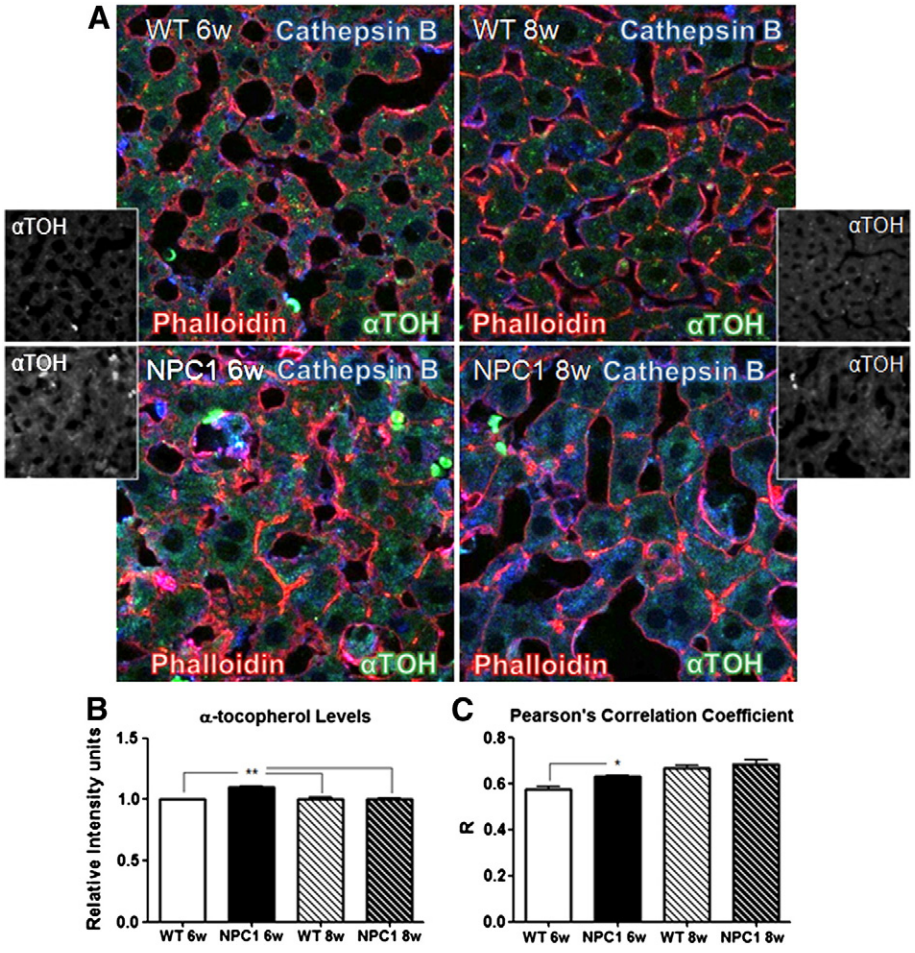

Fig. 5. Immunofluorescence analysis for α-tocopherol signal in livers of WT and NPC1 mice. A. Representative immunofluorescence images for α-TOH (green), cathepsin B (blue) and phalloidin (red) in livers of wild-type (WT) and *Npc1*$^{-/-}$ (NPC1) mice of 6 and 8 week-old (6w and 8w). The black and white image shows the α-TOH signal alone. Image size: 3.7 pixels/nm. B. Quantitation of α-TOH relative levels in livers of 6 and 8 week-old (6w and 8w) WT and NPC1 mice. C. Quantitation of α-TOH and cathepsin B signals co-localization by Pearson's correlation coefficient. Results are shown as mean ± SEM. * $p<0.05$; ** $p<0.01$.

cerebellum of 12 week-old NPC2 mice. In addition, our results indicate an increment of 50% in vitamin E content in the cerebellum at 8 week-old NPC1 animals, age at which the animals clearly show locomotor deterioration, suggesting that bioavailability of vitamin E could be contributing to the cerebellum pathology.

Although NPC1 mice at 6 weeks of age showed increased hepatic levels of α-TOH, we did not find significant differences in the liver between WT and NPC1 mice at 8 weeks of age. This could be due to the progressive liver damage, almost undetectable at 6 weeks of age, but that at 8 weeks is evident by collagen accumulation, infiltration of macrophages and elevated levels of plasma ALT (unpublished results from our group and [55,56]). For this reason, the NPC1 mouse liver tissue at 8 weeks of age would be highly impaired, masking the differences that have been detected at 6 weeks of age.

At a subcellular level, lysosomal membranes contain the highest total levels of α-TOH [57] if they are normalized against phosphorus concentration within phospholipids [58]. We showed a relative enrichment of hepatic α-TOH in mitochondria and lysosomes. In NPC1 livers we detected a 50% increment of α-TOH levels in lysosomes compared to mitochondria, whereas no increase was detected in WT lysosomes compared with WT mitochondria. We also detected a 4-fold enrichment of α-TOH levels in NPC1 lysosomes compared

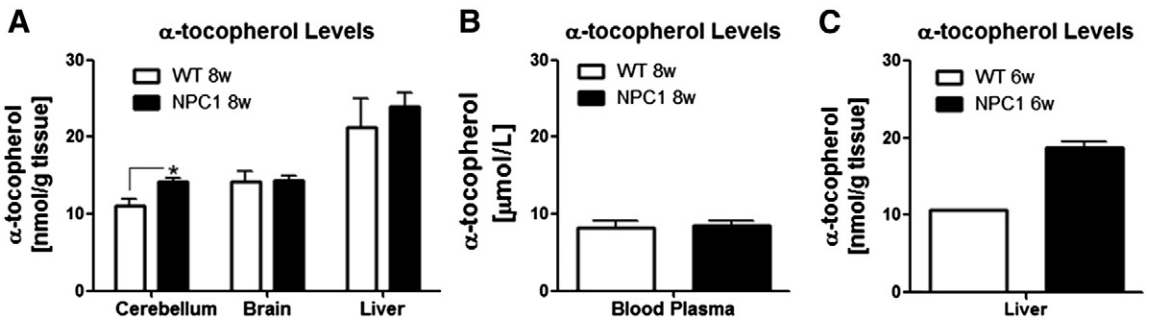

Fig. 6. α-tocopherol content in cerebellum, brain, liver and plasma of WT and NPC1 mice. α-TOH content was measured by HPLC in 8 week-old (8w) WT (n = 4) and NPC1 (n = 7) mice cerebellum, brain and liver (A) and plasma (B), and in livers of 6 week-old (6w) WT (n = 2) and NPC1 (n = 2) mice. Results are shown as mean ± SEM. * $p<0.05$.

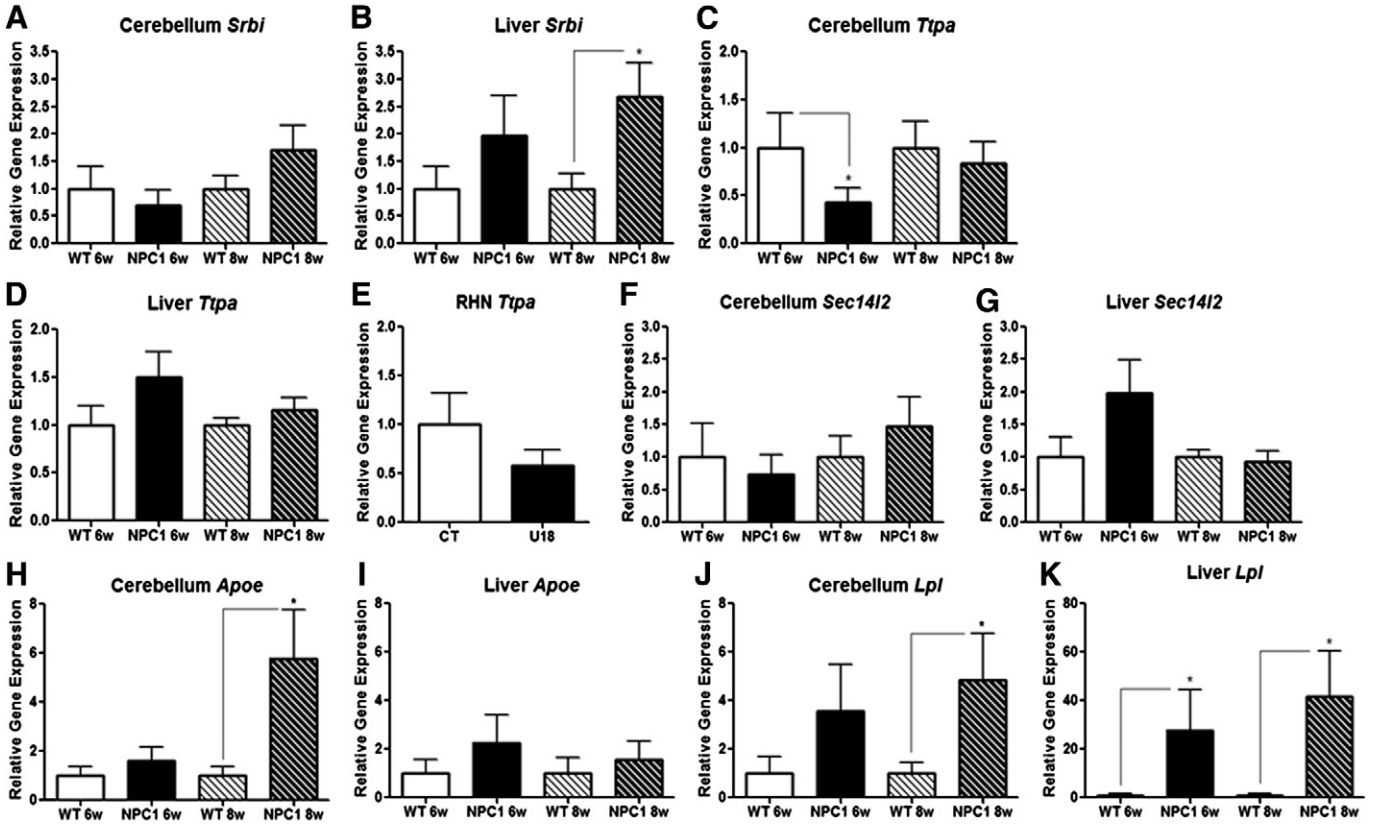

Fig. 7. mRNA expression levels of α-TOH-related genes in rat hippocampal cells and cerebellum and livers of WT and NPC1 mice. The mRNA levels in rat hippocampal cells (RHN) and 6 and 8 week-old WT and NPC1 mice were analyzed by real-time PCR. The gene product was normalized using 18S gene expression. Data are mRNA levels (mean ± SEM values) in rat hippocampal cells and both WT and NPC1 mice. There were 3 untreated and U18-treated rat hippocampal cultures and 4 and 5 mice in each group of 6 and 8 week-old mice, respectively. The following genes were analyzed: α-TOH transfer protein (α-TTP) *Ttpa;* α-TOH associated protein *(Sec14l2)*; lipoprotein transporters, receptors and metabolism-related genes *Apoe*, *Srbi* and *Lpl*; * $p<0.05$ NPC1 vs WT mice.

with the total homogenates, whereas only a 2-fold enrichment was detected in WT lysosomes. In conclusion, our results show a differential localization of hepatic α-TOH with a relative enrichment in NPC1 hepatic lysosomes compared to wild-types.

The results obtained by liver subcellular fractionation were complemented by immunofluorescence and colocalization studies in U18-treated and untreated rat hippocampal neurons. We determined that α-TOH staining mainly colocalize with Lamp1 positive vesicles (a late endosomes/lysosome marker). In this regard, it is important to remark that not all the Lamp1/2 positive vesicles colocalize with NPC proteins [59] which is in agreement with our finding that α-TOH was not present in all Lamp1 positive vesicles as well. U18 treatment increased colocalization between α-TOH and Lamp1 compared to untreated neurons, suggesting that the drug is inducing α-TOH accumulation. Furthermore, we observed colocalization between α-TOH and LysoTracker. Most lysosomes present α-TOH, although the majority of α-TOH was not found within lysosomes.

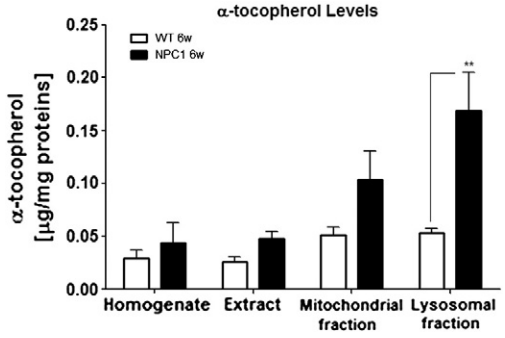

Fig. 8. α-tocopherol content in hepatic subcellular fractions of WT and NPC1 mice. α-TOH content was measured by HPLC in liver fractions of 6 week-old (6w) WT ($n=3$) and NPC1 ($n=3$) mice obtained as described in Materials and methods. Results are shown as mean ± SEM. ** $p<0.01$.

Although U18 has been widely used as an inducer of lipid accumulation in late endomes/lysosomes, it should be mentioned that this agent is toxic at high concentrations and prolonged incubation times [60]. However, under the conditions used in this study for primary hippocampal neurons (0.5 μg/ml for 24 h) no significant differences in cell viability and major morphological changes were observed, as has been reported by Cheung et al. for primary cortical neurons with U18 treatment [60]. In addition, U18 modulates several aspects of cholesterol metabolism besides from triggering lysosomal cholesterol accumulation. It also affects the activity of HMG-CoA reductase, the cholesterol synthesis rate-limiting enzyme, in a concentration-dependent manner [61,62]. Therefore, it cannot be completely ruled out that accumulation of α-TOH in lysosomes of neurons treated with U18 is due, in part, to the effect of the drug on the inhibition of cholesterol synthesis. In this sense, it is possible to speculate that a decrease in cholesterol synthesis, an important source of cholesterol in neurons, would decrease the concentration of cholesterol in the plasma membrane. Given the lipophilic properties of α-TOH it distributes into lipid storage organelles and cell membranes [63]; therefore, inhibition of cholesterol synthesis induced by U18 may indirectly favor the redistribution of α-TOH to the lysosome, which is enriched in cholesterol. Because of this limitation it was necessary to corroborate the results obtained with the pharmacological model of NPC in primary cultured neurons from NPC1 mice, a much more difficult model to work with, in which we also found increments in the α-TOH signal.

To associate NPC α-TOH accumulation with its intracellular trafficking alterations, we measured the transcript levels of several genes related with α-TOH transport and metabolism. Our results show a significant reduction in the *Ttpa* cerebellar mRNA levels, but no differences were found in U18-treated neurons compared with controls. Previous reports show regulation of α-TTP protein levels by α-TOH, however little is known about the regulation of mRNA levels. Patients from neurodegenerative diseases with engagement of oxidative stress such as Alzheimer Disease and AVED present higher α-TTP protein levels [64]. On the other hand, mice fed with a high vitamin E diet show increments in protein levels of α-TTP. In the liver, our results show no significant differences in *Ttpa* mRNA levels between WT and NPC1 mice; even though hepatic α-TOH levels were higher at 6 week-old NPC1 animals. Thus, it seems that alterations in the expression of the α-TTP intracellular transporter are not responsible for a common mechanism for vitamin E accumulation in the cerebellum and liver of NPC1 animals. Higher mRNA expression levels of *Srbi, Apoe* and *Lpl* correlated with α-TOH levels on liver and/or cerebellum. These results suggest that there is an increase uptake and transport of α-TOH in the NPC1 mice but they do not explain its intracellular accumulation as they can neither explain the intracellular accumulation of cholesterol and other lipids. The cerebellum is one of the most susceptible organs to vitamin E deficiency due to high levels of lipid peroxidation. Several metabolic ataxias are caused by malfunction of proteins involved in α-TOH trafficking. Among them is AVED syndrome in which patients can absorb vitamin E correctly, so patients are supplemented with it as part of their treatment. In NPC disease there is a progressive loss of locomotor skills, ataxia, which strongly correlates with early degeneration of Purkinje cells. In the cerebellar cortex, clusters of α-TTP are aligned within small cells around the Purkinje cell layer [65]. This observation together with our results, suggest that vitamin E accumulation and its eventual reduced bioavailability in NPC neurons could initially affect the cerebellum and account for the increased susceptibility of this tissue in the disease. Thus, it is possible to speculate that vitamin E accumulation could have an important pathogenic role in NPC disease and contribute to oxidative damage and cell death.

However, we cannot discard a different scenario in which the excess of vitamin E acts as a pro-oxidant molecule in NPC cells. In fact, α-TOH can play diverse roles in lipoprotein oxidation displaying neutral, anti-, or, indeed, pro-oxidant activity under various conditions [66]. For example, in the presence of determinant Cu^{2+}/LDL ratios α-TOH acts as a mediator of LDL lipid peroxidation [67]. In this sense, it is important to mention that NPC lysosomes accumulate not only cholesterol but also Cu^{2+} [68,69] (unpublished results from our group). Therefore, an alternative hypothesis is that the lysosomal buildup of vitamin E found in NPC cells could actively contribute to the pathology acting as a pro-oxidant molecule and increasing the levels of toxic cholesterol oxidation products. Indeed, there is an increase in the levels of cholesterol oxidation products in plasma and tissues of NPC mice and patients [29,49]. Moreover, a correlation between the oxysterol profile with the age of disease onset and disease severity was established in NPC mice and decreased levels of oxysterols were found in response to therapeutic intervention in the NPC1 feline model [49] suggesting that cholesterol oxidation products could serve as biomarkers of NPC disease. Nevertheless, considering all the above exposed data and our results we think that it is the lower bioavailability of vitamin E which is decreasing the antioxidant defenses in the disease and contributing by this way to the increase in oxidative damage.

NPC cells accumulate cholesterol along with excess sphingomyelin (SM), glycosphingolipids, bis- (monoacylglycerol) phosphate (BMP) [70–72] and other lipids. Therefore, the accumulation and trafficking defects of these other lipids could potentially modulate α-TOH intracellular trafficking. Although the arrangement of vitamin E in biological membranes is presently unknown, considerable information available from studies of model membrane systems show that α-TOH intercalates into phospholipid bilayers with the long axis of the molecule oriented parallel to the lipid hydrocarbon chains [63]. Other indirect evidence suggest that α-TOH interacts, in similar manner as cholesterol with membranes, showing high affinity for sphingomyelin and the fatty acid chains of complex lipids [73]. Thus, it is conceivable that α-TOH intracellular trafficking will be also altered by accumulation of these kinds of lipids in late endosomes/lysosomes from NPC cells.

In addition, sphingolipids accumulation could also exacerbate the susceptibility of NPC cells to oxidative damage. These lipids are regulators of cellular redox homeostasis modulating NADPH oxidase [74], antioxidant enzymes (like catalase) [75] and NOS activity [76]. Therefore, their lower bioavailability could increase oxidative damage in NPC cells.

Despite the increase in oxidative stress, vitamin E treatments did not improve the neurological symptoms of NPC1 mice [28]. Taken together these evidences suggest that vitamin E administration is not able to compensate the oxidative damage of NPC cells, which could be due to the lack of bioavailability of this cellular antioxidant or alternatively, because it is acting as a pro-oxidant molecule.

NPC proteins are capable of transporting other lipids besides cholesterol. This observation, together to the fact that NPC cells accumulate α-TOH within lysosomes, raises the question of whether these proteins are able to directly transport α-TOH. NPC1 protein has a greater affinity for oxysterols than cholesterol [77] and it also shares structural homology with NPC1L1 [37]. Interestingly, NPC1L1 can bind and transport α-TOH, which is inhibited by ezetimibe, suggesting that NPC1L1 α-TOH binding site is the same domain where it binds cholesterol [41,42]. On the other hand, NPC2 has a hydrophobic pocket that binds cholesterol and other sterols as well (cholesterol precursors, oxysterols, etc.) through the saturated hydrocarbons tail [78,79]. However, recent published results show that NPC1 and NPC2 sterol binding domains can bind α-TOH with low affinity, suggesting that the buildup of α-TOH in NPC cells is not due to direct transport impairments but rather by dysfunction of the final stage of the endocytic pathway [23]. Our findings suggest a lower bioavailability of vitamin E, which could have a pathogenic role in disease progression and may contribute to oxidative damage in NPC cells.

Acknowledgments

This study was supported by grants from the Fondo Nacional de Desarrollo Científico y Tecnológico (FONDECYT) (grant numbers 1080221 to A.R.A, and 1070622 and 1110310 to S.Z) and FONDAP 15090007. The authors thank the Humbolt Foundation for the donation of the Applied Biosystems AB7500 real-time PCR machine to the Departamento de Gastroenterología, Facultad de Medicina, Pontificia Universidad Católica de Chile.

Appendix A. Supplementary data

Supplementary data to this article can be found online at doi:10.1016/j.bbadis.2011.11.009.

References

[1] M.C. Patterson, M.T. Vanier, K. Suzuki, J.A. Morris, E.D. Carstea, E.B. Neufeld, E.J. Blanchette-Mackie, P.G. Pentchev, Niemann–Pick disease type C: a lipid trafficking disorder, in: D. Valle, A.L. Beaudet, B. Vogelstein, K.W. Kinzler, S.E. Antonarakis, A. Ballabio, C.R. Scriver, B. Childs, W.S. Sly (Eds.), The Online Metabolic and Molecular Bases of Inherited Disease, McGraw-Hill, New York, 2007, pp. 1–44.
[2] G. Millat, C. Marcais, C. Tomasetto, K. Chikh, A.H. Fensom, K. Harzer, D.A. Wenger, K. Ohno, M.T. Vanier, Niemann–Pick C1 disease: correlations between NPC1 mutations, levels of NPC1 protein, and phenotypes emphasize the functional significance of the putative sterol-sensing domain and of the cysteine-rich luminal loop, Am. J. Hum. Genet. 68 (2001) 1373–1385.
[3] N. Ohgami, D.C. Ko, M. Thomas, M.P. Scott, C.C. Chang, T.Y. Chang, Binding between the Niemann–Pick C1 protein and a photoactivatable cholesterol analog

requires a functional sterol-sensing domain, Proc. Natl. Acad. Sci. U. S. A. 101 (2004) 12473–12478.
[4] E.E. Millard, S.E. Gale, N. Dudley, J. Zhang, J.E. Schaffer, D.S. Ory, The sterol-sensing domain of the Niemann–Pick C1 (NPC1) protein regulates trafficking of low density lipoprotein cholesterol, J. Biol. Chem. 280 (2005) 28581–28590.
[5] A.B. Munkacsi, A.F. Porto, S.L. Sturley, Niemann–Pick type C disease proteins: orphan transporters or membrane rheostats? Future Lipidol. 2 (2007) 357–367.
[6] L. Liscum, J.R. Faust, Low density lipoprotein (LDL)-mediated suppression of cholesterol synthesis and LDL uptake is defective in Niemann–Pick type C fibroblasts, J. Biol. Chem. 262 (1987) 17002–17008.
[7] L. Liscum, R.M. Ruggiero, J.R. Faust, The intracellular transport of low density lipoprotein-derived cholesterol is defective in Niemann–Pick type C fibroblasts, J. Cell Biol. 108 (1989) 1625–1636.
[8] M.T. Vanier, C. Rodriguez-Lafrasse, R. Rousson, N. Gazzah, M.C. Juge, P.G. Pentchev, A. Revol, P. Louisot, Type C Niemann–Pick disease: spectrum of phenotypic variation in disruption of intracellular LDL-derived cholesterol processing, Biochim. Biophys. Acta 1096 (1991) 328–337.
[9] M.C. Patterson, P.G. Pentchev, Diagnosis of Niemann–Pick disease type C, J. Pediatr. 124 (1994) 655–656.
[10] D.S. Ory, Niemann–Pick type C: a disorder of cellular cholesterol trafficking, Biochim. Biophys. Acta 1529 (2000) 331–339.
[11] S.C. Patel, S. Suresh, U. Kumar, C.Y. Hu, A. Cooney, E.J. Blanchette-Mackie, E.B. Neufeld, R.C. Patel, R.O. Brady, Y.C. Patel, P.G. Pentchev, W.Y. Ong, Localization of Niemann-Pick C1 protein in astrocytes: implications for neuronal degeneration in Niemann–Pick type C disease, Proc. Natl. Acad. Sci. U. S. A. 96 (1999) 1657–1662.
[12] M. Taniguchi, Y. Shinoda, H. Ninomiya, M.T. Vanier, K. Ohno, Sites and temporal changes of gangliosides GM1/GM2 storage in the Niemann–Pick disease type C mouse brain, Brain Dev. 23 (2001) 414–421.
[13] M. Zervas, K. Dobrenis, S.U. Walkley, Neurons in Niemann–Pick disease type C accumulate gangliosides as well as unesterified cholesterol and undergo dendritic and axonal alterations, J. Neuropathol. Exp. Neurol. 60 (2001) 49–64.
[14] C.A. Paul, A.K. Boegle, R.A. Maue, Before the loss: neuronal dysfunction in Niemann–Pick Type C disease, Biochim. Biophys. Acta 1685 (2004) 63–76.
[15] S.U. Walkley, K. Suzuki, Consequences of NPC1 and NPC2 loss of function in mammalian neurons, Biochim. Biophys. Acta 1685 (2004) 48–62.
[16] J.V. Reddy, I.G. Ganley, S.R. Pfeffer, Clues to neuro-degeneration in Niemann–Pick type C disease from global gene expression profiling, PLoS One 1 (2006) e19.
[17] M.J. Elrick, C.D. Pacheco, T. Yu, N. Dadgar, V.G. Shakkottai, C. Ware, H.L. Paulson, A.P. Lieberman, Conditional Niemann–Pick C mice demonstrate cell autonomous Purkinje cell neurodegeneration, Hum. Mol. Genet. 19 (2010) 837–847.
[18] C.M. Hawes, H. Wiemer, S.R. Krueger, B. Karten, Pre-synaptic defects of NPC1-deficient hippocampal neurons are not directly related to plasma membrane cholesterol, J. Neurochem. 114 (2010) 311–322.
[19] A.R. Alvarez, A. Klein, J. Castro, G.I. Cancino, J. Amigo, M. Mosqueira, L.M. Vargas, L.F. Yevenes, F.C. Bronfman, S. Zanlungo, Imatinib therapy blocks cerebellar apoptosis and improves neurological symptoms in a mouse model of Niemann–Pick type C disease, FASEB J. 22 (2008) 3617–3627.
[20] A. Klein, C. Maldonado, L.M. Vargas, M. Gonzalez, F. Robledo, K. Perez de Arce, F.J. Muñoz, C. Hetz, A.R. Alvarez, S. Zanlungo, Oxidative stress activates the c-Abl/p73 proapoptotic pathway in Niemann–Pick type C neurons, Neurobiol. Dis. 41 (2011) 209–218.
[21] G.W. Burton, M.G. Traber, Vitamin E: antioxidant activity, biokinetics, and bioavailability, Annu. Rev. Nutr. 10 (1990) 357–382.
[22] A. Hosomi, M. Arita, Y. Sato, C. Kiyose, T. Ueda, O. Igarashi, H. Arai, K. Inoue, Affinity for α-tocopherol transfer protein as a determinant of the biological activities of vitamin E analogs, FEBS Lett. 409 (1997) 105–108.
[23] L. Ulatowski, R. Parker, C. Davidson, N. Yanjanin, T. Kelly, D. Corey, J. Atkinson, F. Porter, H. Arai, S. Walkley, D. Manor, Altered vitamin E status in Niemann–Pick type C disease, J. Lipid Res. 52 (2011) 1400–1410.
[24] S.L. Cuddihy, S.S. Ali, E.S. Musiek, J. Lucero, S.J. Kopp, J.D. Morrow, L.L. Dugan, Prolonged α-tocopherol deficiency decreases oxidative stress and unmasks α-tocopherol-dependent regulation of mitochondrial function in the brain, J. Biol. Chem. 283 (2008) 6915–6924.
[25] K. Ouahchi, M. Arita, H. Kayden, F. Hentati, M. Ben Hamida, R. Sokol, H. Arai, K. Inoue, J.L. Mandel, M. Koenig, Ataxia with isolated vitamin E deficiency is caused by mutations in the α-tocopherol transfer protein, Nat. Genet. 9 (1995) 141–145.
[26] F. Palau, C. Espinos, Autosomal recessive cerebellar ataxias, Orphanet J. Rare Dis. 1 (2006) 47.
[27] T. Yokota, K. Igarashi, T. Uchihara, K. Jishage, H. Tomita, A. Inaba, Y. Li, M. Arita, H. Suzuki, H. Mizusawa, H. Arai, Delayed-onset ataxia in mice lacking α-tocopherol transfer protein: model for neuronal degeneration caused by chronic oxidative stress, Proc. Natl. Acad. Sci. U. S. A. 98 (2001) 15185–15190.
[28] E.C. Bascuñan-Castillo, R.P. Erickson, C.M. Howison, R.J. Hunter, R.H. Heidenreich, C. Hicks, T.P. Trouard, R.J. Gillies, Tamoxifen and vitamin E treatments delay symptoms in the mouse model of Niemann–Pick C, J. Appl. Genet. 45 (2004) 461–467.
[29] R. Fu, N.M. Yanjanin, S. Bianconi, W.J. Pavan, F.D. Porter, Oxidative stress in Niemann–Pick disease type C, Mol. Genet. Metab. 101 (2010) 214–218.
[30] Y. Sato, H. Arai, A. Miyata, S. Tokita, K. Yamamoto, T. Tanabe, K. Inoue, Primary structure of α-tocopherol transfer protein from rat liver. Homology with cellular retinaldehyde-binding protein, J. Biol. Chem. 268 (1993) 17705–17710.
[31] J.F. Oram, A.M. Vaughan, R. Stocker, ATP-binding cassette transporter A1 mediates cellular secretion of α-tocopherol, J. Biol. Chem. 276 (2001) 39898–39902.
[32] P. Mardones, P. Strobel, S. Miranda, F. Leighton, V. Quinones, L. Amigo, J. Rozowski, M. Krieger, A. Rigotti, Alpha-tocopherol metabolism is abnormal in scavenger receptor class B type I (SR-BI)-deficient mice, J. Nutr. 132 (2002) 443–449.
[33] J. Qian, S. Morley, K. Wilson, P. Nava, J. Atkinson, D. Manor, Intracellular trafficking of vitamin E in hepatocytes: the role of tocopherol transfer protein, J. Lipid Res. 46 (2005) 2072–2082.
[34] K. Anwar, H.J. Kayden, M.M. Hussain, Transport of vitamin E by differentiated Caco-2 cells, J. Lipid Res. 47 (2006) 1261–1273.
[35] E. Reboul, A. Klein, F. Bietrix, B. Gleize, C. Malezet-Desmoulins, M. Schneider, A. Margotat, L. Lagrost, X. Collet, P. Borel, Scavenger receptor class B type I (SR-BI) is involved in vitamin E transport across the enterocyte, J. Biol. Chem. 281 (2006) 4739–4745.
[36] E. Reboul, D. Trompier, M. Moussa, A. Klein, J.F. Landrier, G. Chimini, P. Borel, ATP-binding cassette transporter A1 is significantly involved in the intestinal absorption of α- and γ-tocopherol but not in that of retinyl palmitate in mice, Am. J. Clin. Nutr. 89 (2009) 177–184.
[37] J.P. Davies, Y.A. Ioannou, Topological analysis of Niemann–Pick C1 protein reveals that the membrane orientation of the putative sterol-sensing domain is identical to those of 3-hydroxy-3-methylglutaryl-CoA reductase and sterol regulatory element binding protein cleavage-activating protein, J. Biol. Chem. 275 (2000) 24367–24374.
[38] S.W. Altmann, H.R. Davis Jr., L.J. Zhu, X. Yao, L.M. Hoos, G. Tetzloff, S.P. Iyer, M. Maguire, A. Golovko, M. Zeng, L. Wang, N. Murgolo, M.P. Graziano, Niemann–Pick C1 like 1 protein is critical for intestinal cholesterol absorption, Science 303 (2004) 1201–1204.
[39] H.R. Davis Jr., S.W. Altmann, Niemann–Pick C1 Like 1 (NPC1L1) an intestinal sterol transporter, Biochim. Biophys. Acta 1791 (2009) 679–683.
[40] M. Garcia-Calvo, J. Lisnock, H.G. Bull, B.E. Hawes, D.A. Burnett, M.P. Braun, J.H. Crona, H.R. Davis Jr., D.C. Dean, P.A. Detmers, M.P. Graziano, M. Hughes, D.E. Macintyre, A. Ogawa, K.A. O'neill, S.P. Iyer, D.E. Shevell, M.M. Smith, Y.S. Tang, A.M. Makarewicz, F. Ujjainwalla, S.W. Altmann, K.T. Chapman, N.A. Thornberry, The target of ezetimibe is Niemann–Pick C1-Like 1 (NPC1L1), Proc. Natl. Acad. Sci. U. S. A. 102 (2005) 8132–8137.
[41] K. Narushima, T. Takada, Y. Yamanashi, H. Suzuki, Niemann–Pick C1-like 1 mediates α-tocopherol transport, Mol. Pharmacol. 74 (2008) 42–49.
[42] A.B. Weinglass, M. Kohler, U. Schulte, J. Liu, E.O. Nketiah, A. Thomas, W. Schmalhofer, B. Williams, W. Bildl, D.R. McMasters, K. Dai, L. Beers, M.E. McCann, G.J. Kaczorowski, M.L. Garcia, Extracellular loop C of NPC1L1 is important for binding to ezetimibe, Proc. Natl. Acad. Sci. U. S. A. 105 (2008) 11140–11145.
[43] L. Amigo, H. Mendoza, J. Castro, V. Quinones, J.F. Miquel, S. Zanlungo Relevance, of Niemann–Pick type C1 protein expression in controlling plasma cholesterol and biliary lipid secretion in mice, Hepatology 36 (2002) 819–828.
[44] A.R. Alvarez, P.C. Sandoval, N.R. Leal, P.U. Castro, K.S. Kosik, Activation of the neuronal c-Abl tyrosine kinase by amyloid-beta-peptide and reactive oxygen species, Neurobiol. Dis. 17 (2004) 326–336.
[45] M.W. Pfaffl, A new mathematical model for relative quantification in real-time RT-PCR, Nucleic Acids Res. 29 (2001) e45.
[46] M.M. Bradford, A rapid and sensitive method for the quantitation of microgram quantities of protein utilizing the principle of protein–dye binding, Anal. Biochem. 72 (1976) 248–254.
[47] P.A. Motchnik, B. Frei, B.N. Ames, Measurement of antioxidants in human blood plasma, Methods Enzymol. 234 (1994) 269–279.
[48] B. Karten, D.E. Vance, R.B. Campenot, J.E. Vance, Cholesterol accumulates in cell bodies, but is decreased in distal axons, of Niemann–Pick C1-deficient neurons, J. Neurochem. 83 (2002) 1154–1163.
[49] F.D. Porter, D.E. Scherrer, M.H. Lanier, S.J. Langmade, V. Molugu, S.E. Gale, D. Olzeski, R. Sidhu, D.J. Dietzen, R. Fu, C.A. Wassif, N.M. Yanjanin, S.P. Marso, J. House, C. Vite, J.E. Schaffer, D.S. Ory, Cholesterol oxidation products are sensitive and specific blood-based biomarkers for Niemann–Pick C1 disease, Sci. Transl. Med. 2 (2010) 56ra81.
[50] J.M. Zingg, P. Kempna, M. Paris, E. Reiter, L. Villacorta, R. Cipollone, A. Munteanu, C. De Pascale, S. Menini, A. Cueff, M. Arock, A. Azzi, R. Ricciarelli, Characterization of three human sec14p-like proteins: alpha-tocopherol transport activity and expression pattern in tissues, Biochimie 90 (2008) 1703–1715.
[51] H. Li, J.J. Repa, M.A. Valasek, E.P. Beltroy, S.D. Turley, D.C. German, J.M. Dietschy, Molecular, anatomical, and biochemical events associated with neurodegeneration in mice with Niemann–Pick type C disease, J. Neuropathol. Exp. Neurol. 64 (2005) 323–333.
[52] H. Hayashi, Lipid metabolism and glial lipoproteins in the central nervous system, Biol. Pharm. Bull. 34 (2011) 453–461.
[53] C. Abe, S. Ikeda, T. Uchida, K. Yamashita, T. Ichikawa, Triton WR1339, an inhibitor of lipoprotein lipase, decreases vitamin E concentration in some tissues of rats by inhibiting its transport to liver, J. Nutr. 137 (2007) 345–350.
[54] D.H. Bessesen, C.L. Richards, J. Etienne, J.W. Goers, R.H. Eckel, Spinal cord of the rat contains more lipoprotein lipase than other brain regions, J. Lipid Res. 34 (1993) 229–238.
[55] V.M. Rimkunas, M.J. Graham, R.M. Crooke, L. Liscum, In vivo antisense oligonucleotide reduction of NPC1 expression as a novel mouse model for Niemann Pick type C-associated liver disease, Hepatology 47 (2008) 1504–1512.
[56] E.P. Beltroy, B. Liu, J.M. Dietschy, S.D. Turley, Lysosomal unesterified cholesterol content correlates with liver cell death in murine Niemann–Pick type C disease, J. Lipid Res. 48 (2007) 869–881.
[57] C.A. Rupar, S. Albo, J.D. Whitehall, Rat liver lysosome membranes are enriched in α-tocopherol, Biochem. Cell Biol. 70 (1992) 486–488.
[58] J.L. Buttriss, A.T. Diplock, The relationship between α-tocopherol and phospholipid fatty acids in rat liver subcellular membrane fractions, Biochim. Biophys. Acta 962 (1988) 81–90.
[59] E.B. Neufeld, M. Wastney, S. Patel, S. Suresh, A.M. Cooney, N.K. Dwyer, C.F. Roff, K. Ohno, J.A. Morris, E.D. Carstea, J.P. Incardona, J.F. Strauss III, M.T. Vanier, M.C.

Patterson, R.O. Brady, P.G. Pentchev, E.J. Blanchette-Mackie, The Niemann–Pick C1 protein resides in a vesicular compartment linked to retrograde transport of multiple lysosomal cargo, J. Biol. Chem. 274 (1999) 9627–9635.
[60] N.S. Cheung, C.H. Koh, B.H. Bay, R.Z. Qi, M.S. Choy, Q.T. Li, K.P. Wong, M. Whiteman, Chronic exposure to U18666A induces apoptosis in cultured murine cortical neurons, Biochem. Biophys. Res. Commun. 315 (2004) 408–417.
[61] A. Boogaard, M. Griffioen, L.H. Cohen, Regulation of 3-hydroxy-3-methylglutaryl-coenzyme A reductase in human hepatoma cell line Hep G2. Effects of inhibitors of cholesterol synthesis on enzyme activity, Biochem. J. 241 (1987) 345–351.
[62] Y. Lange, T.L. Steck, Cholesterol homeostasis. Modulation by amphiphiles, J. Biol. Chem. 269 (1994) 29371–29374.
[63] X. Wang, P.J. Quinn, Vitamin E and its function in membranes, Prog. Lipid Res. 38 (1999) 309–336.
[64] R.P. Copp, T. Wisniewski, F. Hentati, A. Larnaout, H.M. Ben, H.J. Kayden, Localization of α-tocopherol transfer protein in the brains of patients with ataxia with vitamin E deficiency and other oxidative stress related neurodegenerative disorders, Brain Res. 822 (1999) 80–87.
[65] A. Hosomi, K. Goto, H. Kondo, T. Iwatsubo, T. Yokota, M. Ogawa, M. Arita, J. Aoki, H. Arai, K. Inoue, Localization of α-tocopherol transfer protein in rat brain, Neurosci. Lett. 256 (1998) 159–162.
[66] D.J. Mustacich, S.W. Leonard, N.K. Patel, M.G. Traber, Alpha-tocopherol beta-oxidation localized to rat liver mitochondria, Free Radic. Biol. Med. 48 (2010) 73–81.
[67] J.M. Upston, A.C. Terentis, R. Stocker, Tocopherol-mediated peroxidation of lipoproteins: implications for vitamin E as a potential antiatherogenic supplement, FASEB J. 13 (1999) 977–994.
[68] C. Yanagimoto, M. Harada, H. Kumemura, H. Koga, T. Kawaguchi, K. Terada, S. Hanada, E. Taniguchi, Y. Koizumi, S. Koyota, H. Ninomiya, T. Ueno, T. Sugiyama, M. Sata, Niemann–Pick C1 protein transports copper to the secretory compartment from late endosomes where ATP7B resides, Exp. Cell Res. 315 (2009) 119–126.
[69] C. Yanagimoto, M. Harada, H. Kumemura, M. Abe, H. Koga, M. Sakata, T. Kawaguchi, K. Terada, S. Hanada, E. Taniguchi, H. Ninomiya, T. Ueno, T. Sugiyama, M. Sata, Copper incorporation into ceruloplasmin is regulated by Niemann–Pick C1 protein, Hepatol. Res. 41 (2011) 484–491.
[70] V. Puri, R. Watanabe, M. Dominguez, X. Sun, C.L. Wheatley, D.L. Marks, R.E. Pagano, Cholesterol modulates membrane traffic along the endocytic pathway in sphingolipid-storage diseases, Nat. Cell Biol. 1 (1999) 386–388.
[71] B. Karten, K.B. Peake, J.E. Vance, Mechanisms and consequences of impaired lipid trafficking in Niemann–Pick type C1-deficient mammalian cells, Biochim. Biophys. Acta 1791 (2009) 659–670.
[72] J. Chevallier, Z. Chamoun, G. Jiang, G. Prestwich, N. Sakai, S. Matile, R.G. Parton, J. Gruenberg, Lysobisphosphatidic acid controls endosomal cholesterol levels, J. Biol. Chem. 283 (2008) 27871–27880.
[73] S.K. Noh, S.I. Koo, Egg sphingomyelin lowers the lymphatic absorption of cholesterol and alpha-tocopherol in rats, J. Nutr. 133 (2003) 3571–3576.
[74] D.X. Zhang, A.P. Zou, P.L. Li, Ceramide-induced activation of NADPH oxidase and endothelial dysfunction in small coronary arteries, Am. J. Physiol. Heart Circ. Physiol. 284 (2003) H605–H612.
[75] K. Iwai, T. Kondo, M. Watanabe, T. Yabu, T. Kitano, Y. Taguchi, H. Umehara, A. Takahashi, T. Uchiyama, T. Okazaki, Ceramide increases oxidative damage due to inhibition of catalase by caspase-3-dependent proteolysis in HL-60 cell apoptosis, J. Biol. Chem. 278 (2003) 9813–9822.
[76] P. Viani, P. Giussani, A. Ferraretto, A. Signorile, L. Riboni, G. Tettamanti, Nitric oxide production in living neurons is modulated by sphingosine: a fluorescence microscopy study, FEBS Lett. 506 (2001) 185–190.
[77] R.E. Infante, L. Abi-Mosleh, A. Radhakrishnan, J.D. Dale, M.S. Brown, J.L. Goldstein, Purified NPC1 protein. I. Binding of cholesterol and oxysterols to a 1278-amino acid membrane protein, J. Biol. Chem. 283 (2008) 1052–1063.
[78] H.L. Liou, S.S. Dixit, S. Xu, G.S. Tint, A.M. Stock, P. Lobel, NPC2, the protein deficient in Niemann–Pick C2 disease, consists of multiple glycoforms that bind a variety of sterols, J. Biol. Chem. 281 (2006) 36710–36723.
[79] S. Xu, B. Benoff, H.L. Liou, P. Lobel, A.M. Stock, Structural basis of sterol binding by NPC2, a lysosomal protein deficient in Niemann–Pick type C2 disease, J. Biol. Chem. 282 (2007) 23525–23531.